Strojnícky časopis – *Journal of* MECHANICAL ENGINEERING,
VOL 74 (2024), NO 3, 131 - 144

# STUDY ON STICK-SLIP OSCILLATIONS AS A FORMATION MECHANISM OF RAIL CORRUGATION ON METRO LINES AND PARAMETER ANALYSIS

**WANG Zhiqiang [1*], LEI Zhenyu [2]**

[1] *State Key Laboratory of Mechanical Behaviour and System Safety of Traffic Engineering Structures, Shijiazhuang Tiedao University, 050043 Shijiazhuang, China, e-mail: wangzq@tongji.edu.cn*
[2] *Institute of Rail Transit, Tongji University, 201804 Shanghai, China, e-mail: leizhenyu@tongji.edu.cn*

**Abstract:** The objective of the current study is to investigate the formation mechanism of rail corrugation. According to the actual wheel-rail motion relationship, that is, considering the influence of the angle of attack (AoA), a single degree of freedom friction pair model considering different friction attributes was established. The system stick-slip oscillation characteristics under different friction attributes were analyzed by using the model, so as to explore the generation reason of corrugation. Meantime, combined with the parameter analysis of the power system, the corresponding control measures for the stick-slip oscillation were put forward to slow down the formation and development of corrugation. The results show that the lateral and vertical dynamics play important role on its stick-slip oscillation characteristics. The corrugation formation on the metro small radius curve is related to the unstable stick-slip oscillation induced by the negative slope friction creep property of wheel-rail interface. The parameter analysis illustrates that the unstable stick-slip oscillation can be effectively controlled by increasing the damping coefficient, increasing the modal stiffness, appropriately reducing the static vertical force of the contact interface and increasing the lateral velocity (AoA) within a certain range. Practically, knowing the formation mechanism of rail corrugation is conducive to understanding the evolution process of rail corrugation; meantime, by referring to the results of parameter analysis, the active control of stick-slip oscillations can be realized, thereby controlling the growth of rail corrugation.

**KEYWORDS:** Metro; rail corrugation; friction pair model; stick-slip oscillation; parameter analysis.

## 1 Introduction

As the rapid progress of rail transit and the increasing travel demand of people, more and more metro lines have been opened all over the world. Although the running speed of metro vehicles is relatively low, its high running frequency still causes a series of serious diseases on metro lines [1,2], and rail corrugation is one of them. Rail corrugation is a periodical longitudinal wear phenomenon, which is a hard problem to be solved by railway departments. Rail corrugation will exacerbate the component damage and affect the stability of train operation and the surrounding living environment. Slight corrugation can be removed by grinding, but when corrugation is more serious, rail can only be replaced, resulting in a lot of economic investment.

The research on corrugation has lasted for a century, but there are still differences in the understanding of its formation mechanism. Track resonance [3-5] or wheel-rail resonance [6-8] is considered to be the key factor leading to rail corrugation, and the resulting resonance theory can also well explain part of the phenomena of rail corrugation. However, the research methods used, such as modal analysis and Fourier transform, are difficult to determine dominant frequencies directly, which can only be speculated according to field operation situations, and the analysis is subjective. The literatures [9-12] adopt the complex mode

DOI: 10.2478/scjme-2024-0040, Print ISSN 0039-2472, On-line ISSN 2450-5471

theory to determine the characteristic frequencies, and believe that the frequencies promote the generation of rail corrugation. Nevertheless, the specific interaction has not been explained yet, which needs further study. In addition, some literatures [13-16] discuss the generation of corrugation from stick-slip characteristics, and conclude that stick-slip oscillations at the interface induce corrugation. Wheel-rail stick-slip oscillation can explain corrugation formation from the micro level, but the cause of the oscillation has not been determined yet. Some scholars [17-21] believe that fixed defects induce wheel-rail stick-slip oscillations, and then the wave-like wear is formed at the corresponding position and develops continuously. However, fixed defects actually only endowing the phase synchronization characteristic, and appear to be of little concern in generating stick-slip oscillations.

Corrugation is the micro wear behavior, so it is more convincing to study it from micro stick-slip characteristics. The main characteristic of stick-slip phenomena is the nonconstancy of the coefficient of friction (COF) in mechanical systems, that is, the COF in the adhesive state is the static COF, the COF in the sliding state is the dynamic COF, and the dynamic COF is less than the static COF. Since stick-slip phenomena is strongly associated with interface friction attributes, the stick-slip oscillation is probably a result of unstable vibrations arising from interface friction. In view of this, this paper discusses the effect of contact friction attributes on stick-slip oscillations from the micro level, and then explains the formation mechanism of corrugation and analyzes relevant parameter effect.

The structure is as follows: the first section mainly describes the research background; in the second section, by simplifying the actual wheel-rail motion relationship, the friction pair model with single degree of freedom considering different friction attributes is established; in the third section, the stick-slip oscillation under various friction attributes are analyzed by using the friction pair model established, and the corrugation generation is explored; in the fourth section, the factors of damping coefficient, modal stiffness, static vertical force and velocity of the system are investigated, and the corresponding control measures for stick-slip oscillation are put forward to restrain and slow down the generation and development of corrugation; the fifth section summarizes the whole paper. Compared with the existing literatures, the cause of stick-slip oscillation is further clarified in this paper, and the formation mechanism of corrugation on actual lines is interpreted from micro stick-slip characteristics. The conclusions obtained are helpful to comprehensively understand and control the phenomenon of rail corrugation.

## 2 Friction pair model considering different friction attributes

In the metro system, corrugation often appears in the curve section, especially with the decrease of curve radii, the occurrence probability greatly increases [22-25]. When the vehicle operates on a curve track, there will be an AoA $\theta$ formed. The existence of AoA $\theta$ will cause the wheel to generate a lateral velocity $V_1$, as shown in Figure 1. Since the rail is at rest, the lateral velocity represents the wheel-rail relative lateral velocity. When the relative lateral velocity exists, it indicates that the lateral creepage $\varepsilon_1$ has been generated, and the lateral creepage will further induce the lateral force $F_1$, whose direction is opposite to that of the lateral velocity. Meantime, in the process of vehicle operation, the longitudinal relative velocity $V_2$ and the corresponding longitudinal creepage $\varepsilon_2$ and longitudinal force $F_2$ also always exist. When the AoA approaches 0, the above parameters represent the wheel-rail mechanical state on a straight line.

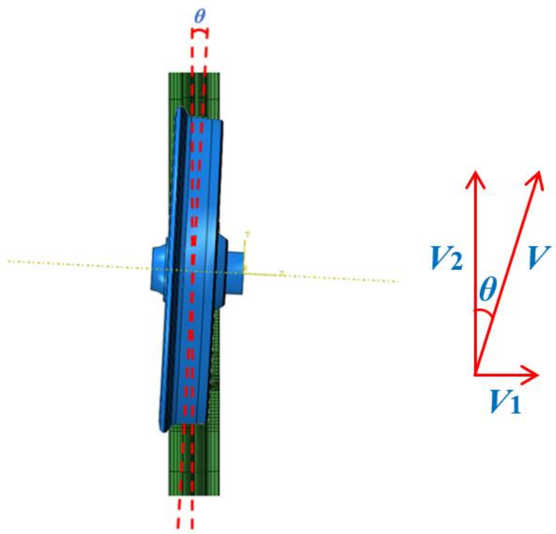


Fig. 1 Diagram of wheel-rail motion relationship

For describing the wheel-rail motion relationship above, a 1-DOF (Degree of Freedom) friction pair model that can consider the friction variation features is established, as shown in Figure 2. This friction pair model can be represented by equation (1) [26],

$$m\ddot{y}(t) + c\dot{y}(t) + ky(t) = F(\varepsilon) \tag{1}$$

where, $m$, $c$ and $k$ are modal mass, damping coefficient and modal stiffness; $F(\varepsilon)$ is the modal force in the contact patch, which can be expressed as,

$$F(\varepsilon) = -\mu(\varepsilon)W \tag{2}$$

where $W$ is the vertical force, consisting of the static force $F_N$ and the dynamic force $F_N(t)$, as shown in equation (3),

$$W(t) = F_N + F_N(t) \tag{3}$$

and the dynamic force $F_N(t)$ is,

$$F_N(t) = A\sin(\omega t) \tag{4}$$

where, $A$ is the variation amplitude; $\omega$ is the angular frequency, and its value is $\sqrt{k/m}$. Thus, the equation (1) can be rewritten as,

$$m\ddot{y}(t) + c\dot{y}(t) + ky(t) = F(\varepsilon, t) \tag{5}$$

In equation (2), $\mu(\varepsilon)$ is the interface adhesion coefficient, which is related to the creepage and can be expressed as [27],

$$\mu(\varepsilon) = \begin{cases} \mu_k \left\{ \varepsilon' - \frac{1}{3}\varepsilon'^2 + \frac{1}{27}\varepsilon'^3 \right\} & for\ \varepsilon' \le 3 \\ \mu_k & for\ \varepsilon' > 3 \end{cases} \tag{6}$$

where $\varepsilon'$ is the nominal creepage, which can be written as,

$$\varepsilon' = \frac{\varepsilon G a b C_{22}}{\mu_0 W} \tag{7}$$

where, $a$ and $b$ are long and short semi-axes of the elliptic contact patch; $G = E/2(1+\upsilon)$, $E$ is the elastic modulus, $\upsilon$ is the Poisson's ratio; $C_{22}$ is a constant with a value of 3.14; $\mu_0$ is the static COF; $\varepsilon$ is the creepage, as shown in equation (8),

$$\varepsilon = [V_1 + \dot{y}(t)]/V \tag{8}$$

where $\dot{y}(t)$ is the lateral vibration velocity of the wheel.

In order to consider the influence of friction attributes on stick-slip oscillations, three kinds of friction creep characteristic curves are established in this section, which are respectively positive slope friction creep curve, zero slope friction creep curve and negative slope friction creep curve. For the positive slope friction creep curve, the $\mu_k$ in equation (6) can be expressed as [28],

$$\mu_k(\varepsilon) = 0.5\mu_0\{2 + e^{-0.138/|\varepsilon V|} + e^{-6.9/|\varepsilon V|}\} \tag{9}$$

For zero slope friction creep curve, the equation (6) can be modified as [29],

$$\mu(\varepsilon) = \begin{cases} \mu_0\left\{\varepsilon' - \frac{1}{3}\varepsilon'^2 + \frac{1}{27}\varepsilon'^3\right\} & for\ \varepsilon' \le 3 \\ \mu_0 & for\ \varepsilon' > 3 \end{cases} \tag{10}$$

The negative slope friction creep curve can be obtained by modifying equation (9), as shown in equation (11),

$$\mu_k(\varepsilon) = 0.5\mu_0\left\{2 - e^{-\frac{0.138}{|\varepsilon V|}} - e^{-6.9/|\varepsilon V|}\right\} \tag{11}$$

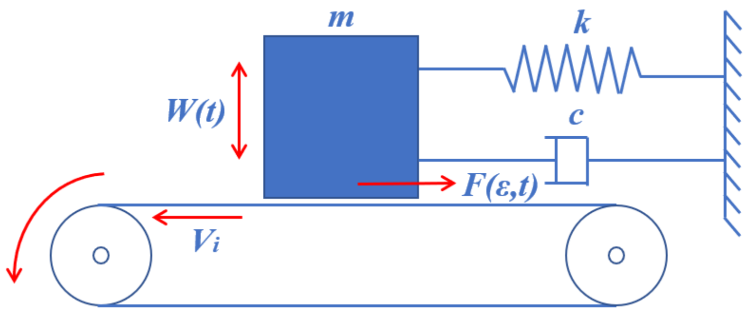


Fig. 2 Friction pair model with single degree of freedom

The parameter values of the 1-DOF friction pair model established above are shown in Table 1 [26,30]. The values of $m$, $c$ and $k$ are obtained by the impact hammer test method; the values of $A$ and $F_N$ are set according to the simulation condition; $E$ and $\upsilon$ are the values of steel material properties; $\mu$ is the value of static COF under the dry condition; and the values of $a$ and $b$ are obtained by the test rig test. In the following, the stick-slip oscillation features under various friction attributes will be analyzed by using this model and combining with the results of literature investigation on rail corrugation.

Table 1 The parameter values of friction pair model.

| **Parameter** | **Value** | **Unit** |
|---|---|---|
| Modal mass $m$ | 0.31 | kg |
| Damping coefficient $c$ | 42 | Ns/m |
| Modal stiffness $k$ | $1.6\times10^8$ | N/m |
| Variation amplitude $A$ | 200 | N |
| Elastic modulus $E$ | 209 | GPa |
| Poisson's ratio $\upsilon$ | 0.27 | - |
| Static COF $\mu_0$ | 0.5 | - |
| Long semi-axe of contact patch $a$ | 0.8378 | mm |
| Short semi-axe of contact patch $b$ | 0.53367 | mm |
| Static vertical force $F_N$ | 200 | N |

## 3 Stick-slip oscillation characteristics of the system

### 3.1 Corrugation investigation

In metro lines, rail corrugation always appears at curve sections with small radii, and the formation of corrugation is primarily associated with the lateral/longitudinal creep and vertical dynamics [13-15,31]. Therefore, for different line types, the variation law of stick-slip oscillation characteristics is studied from the aspects of lateral/longitudinal and vertical interactions of the system. In other words, for the curve section, the effects of lateral and vertical dynamics on stick-slip oscillation characteristics are studied; for the straight section, the effects of longitudinal and vertical dynamics on stick-slip oscillation characteristics are studied. It should be noted that for curve sections, if the effects of longitudinal and vertical dynamics on stick-slip oscillation characteristics is taken into account, the situation is similar to that of the straight section because the AoA is very small. Meantime, the creep force between the wheel and rail is not saturated in straight tracks, therefore, the condition on the straight section is no longer considered in this section.

### 3.2 Stick-slip oscillation characteristics on the curve section

Set the wheel rolling speed $V$ as 16 m/s and the wheel-rail AoA $\theta$ as 0.0045 rad, then according to Figure 1, the calculation equations of wheel-rail relative lateral velocity $V_1$ and wheel-rail relative longitudinal velocity $V_2$ can be written as,

$$\begin{cases} V_1 = V \times \sin\theta \\ V_2 = V \times \cos\theta \end{cases} \tag{12}$$

Through calculation, it can be obtained that $V_1$ is 0.0720 m/s and $V_2$ is 15.9998 m/s. Since corrugation on curve sections is primarily associated with the lateral and vertical dynamics, the influence of $V_1$ on the stick-slip oscillation of the friction pair system is mainly investigated in this section. According to the friction pair model established in Section 2, and using the parameter values shown in Table 1, the horizontal force (the same as the lateral force) $F_1$ borne by the slider, the displacement $y$, the velocity $\dot{y}(t)$ and the acceleration $\ddot{y}(t)$ of the slider are extracted as the output variables. Then, the stick-slip oscillation characteristics under various friction attributes are analyzed. The output variable curves corresponding to the positive, zero and negative slope friction creep conditions are shown in Figure 3. The calculation tool used in this paper is mainly SIMULINK.

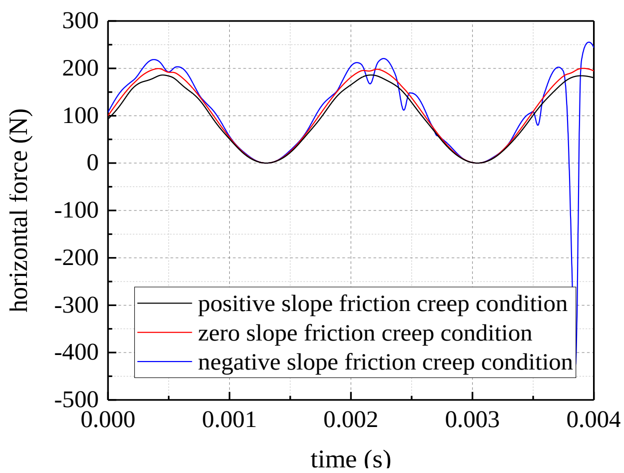


(a) Horizontal force

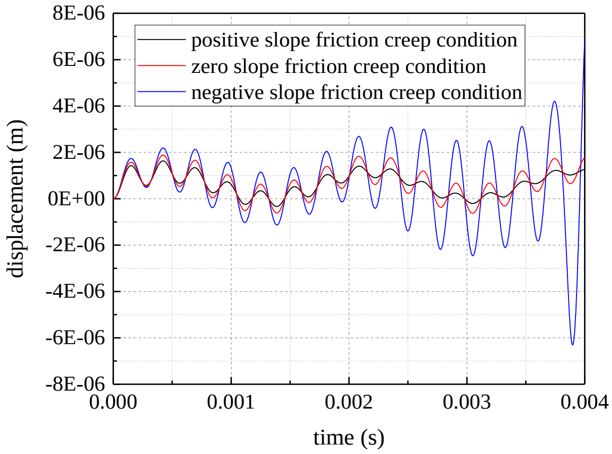


(b) Displacement

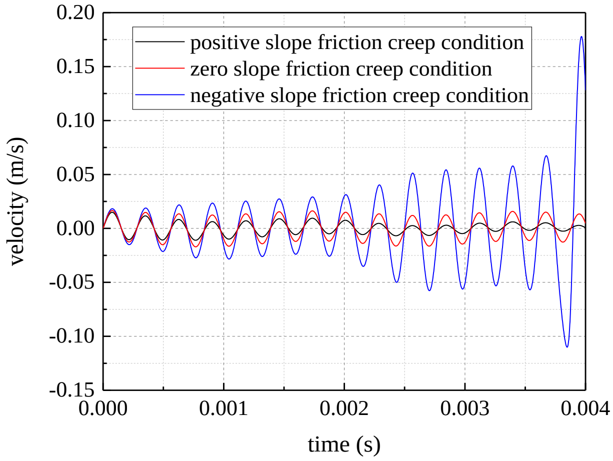


(c) Velocity

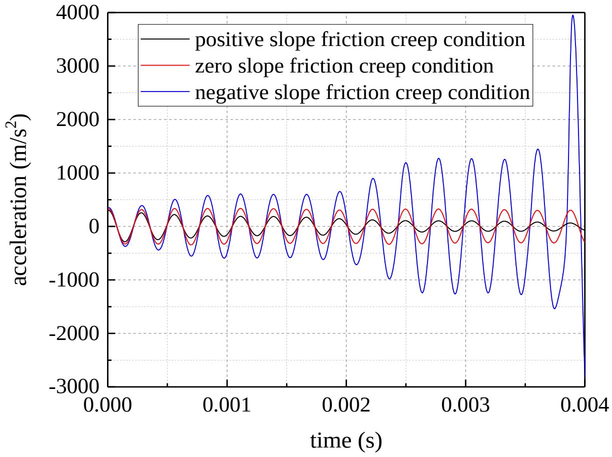


(d) Acceleration

Fig. 3 Output variable curves

According to Figure 3, under the positive slope friction creep condition, the variation amplitude of horizontal force on the slider remains constant, while the variation amplitudes of displacement, velocity and acceleration of the slider gradually decrease with the increase of time and show a convergence trend, indicating that the system gradually tends to be stable; under the zero slope friction creep condition, the variation amplitude of horizontal force on the slider and the variation amplitudes of displacement, velocity and acceleration of the slider all remain constant with the increase of time, indicating that the system is in a stable state; under the negative slope friction creep condition, the variation amplitude of horizontal force on the slider and the variation amplitudes of displacement, velocity and acceleration of the slider all increase gradually with the increase of time and present a divergent trend, indicating that the system is in an unstable oscillation state, which is determined by the negative slope friction creep property of the contact interface. Through the above analysis, it can be obtained that the negative slope friction creep property of the contact interface can induce the unstable stick-slip oscillation, while the positive slope friction creep property and zero slope friction creep property can promote the stability.

Further, by comparing (a), (b), (c) and (d) in Figure 3, it can be seen that, at the fixed time, the variation amplitudes of the system output variables under the zero slope friction creep condition are slightly greater than those under the positive slope friction creep condition, while the variation amplitudes of the system output variables under the negative slope friction creep condition are much larger than those under the other two conditions. Moreover, compared with the zero slope friction creep condition, the output variable amplitude increases by 119% to 1312% under the negative slope friction creep condition, and the output variable amplitude decreases by 6% to 93% under the positive slope friction creep condition. It illustrates that the negative slope friction creep property of the contact interface can amplify the dynamic responses of the system, and it will continue to develop and amplify over time.

It can be concluded from the above that the negative slope friction creep property of the contact interface induces the system to produce unstable stick-slip oscillation, which increases the dynamic responses, while the positive slope friction creep property and zero slope friction creep property promote the system to maintain stability. By extension, in the metro curve section, especially in the sharp curve section, the creep force often reaches saturation [32], so the wheel-rail interface will have a negative slope friction creep property. The existence of negative slope friction creep property will lead to the unstable stick-slip oscillation. If the rail surface has fixed defects, the stick-slip oscillation has the phase synchronization condition. As a result, with the increase of the number of wheel runs, the rail surface will form periodic wavy wear, i.e., rail corrugation. Therefore, the formation of corrugation in the metro curve section is mainly induced by the unstable stick-slip oscillation caused by the negative slope friction creep property. Avoiding the negative slope friction creep property of the contact interface can effectively inhibit the unstable stick-slip oscillation, thereby control the occurrence and evolution of corrugation.

### 3.3 Indoor test analysis

In this section, the effect of various friction attributes on the system response is analyzed using a self-designed twin-disc test rig, as shown in Figure 4. Two main friction attributes are considered, one is the dry friction attribute, i.e., a negative slope friction creep phenomenon can occur; the other is the presence of the water-based friction modifier at the contact interface, i.e., it exhibits a positive slope friction creep behavior, in which the friction modifier is shown in Figure 5. Two groups of tests are set up to simulate the above two kinds of friction attributes, and the running times of tests are both 12 hours. When the test is completed, the wear state on the surface of the rail wheel is observed and recorded, as shown in Figure 6.

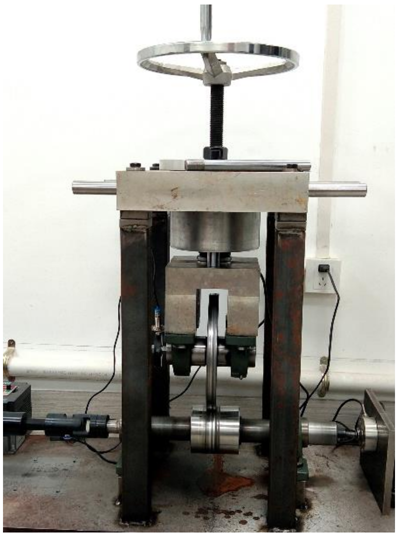

Fig. 4 Twin-disc test rig


Fig. 5 Water-based friction modifier

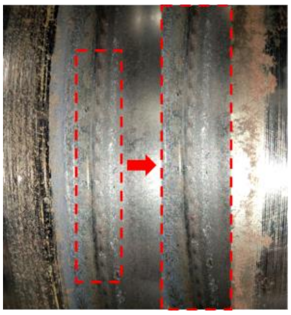

(a) Dry friction condition

(b) Friction modifier condition

Fig. 6 Wear states on rail wheel surfaces

As can be seen from Figure 6, for the dry friction condition, the surface of the rail wheel shows the phenomenon of corrugation; while for the friction modifier condition, the surface of the rail wheel does not show corrugation. The above results indicate that the presence of the friction modifier, i.e., the presence of the positive slope friction creep property, greatly slows down the appearance of corrugation. This agrees well with the results obtained in Section 3.2, thus verifying the validity of numerical calculations.

## 4 System parameter analysis

Taking the dynamic system under the negative slope friction creep condition corresponding to the curve section as an example, this section carries out parameter analysis on the damping coefficient $c$, modal stiffness $k$, static vertical force $F_N$ and lateral velocity $V_1$ (corresponding to the AoA $\theta$), and the corresponding stick-slip oscillation control measures are proposed to manage corrugation. The value range of each variable is shown in Table 2.

Table 2 Value range of each variable for parameter analysis

| **Variable** | **0.8×reference value** | **0.9×reference value** | **reference value** | **1.1×reference value** | **1.2×reference value** |
|---|---|---|---|---|---|
| Damping coefficient $c$/(Ns/m) | 33.6 | 37.8 | 42 | 46.2 | 50.4 |
| Modal stiffness $k$/(N/m) | $1.28\times10^8$ | $1.44\times10^8$ | $1.6\times10^8$ | $1.76\times10^8$ | $1.92\times10^8$ |
| Static vertical force $F_N$/N | 160 | 180 | 200 | 220 | 240 |
| Lateral velocity $V_1$/(m/s) (AoA $\theta$/rad) | 0.0576 (0.0036) | 0.0648 (0.00405) | 0.0720 (0.0045) | 0.0792 (0.00495) | 0.0864 (0.0054) |

The method of parameter analysis used is the control variable method. Firstly, the reference value of each variable is selected as the control variable. Then, under the premise of fixing control variables, the influence of single variable factor on stick-slip oscillation characteristics of the system is studied by changing the value of single variable factor. To facilitate the measurement of the stability of the system's stick-slip oscillation, the vibration power input function $P_{F1}$ of the slider, which takes viscous damping into account, is used to represent the stability of the system, as shown in equation (13),

$$P_{F1} = F_1\dot{y}(t) - \eta(\dot{y}(t))^2 \tag{13}$$

where $\eta$ is the modal damping, which can be expressed as,

$$\eta = 2\zeta\omega m \tag{14}$$

where $\zeta$ is the viscous damping ratio of the system and set as 0.06 according to the impact hammer test. If $P_{F1}$ is positive, it means $F_1$ is putting energy into the system; if $P_{F1}$ is negative, then $F_1$ is dissipating energy in the system. If the sum of the amplitude variations of $P_{F1}$ within a movement period is 0, it illustrates that the system is in a stable state; otherwise, the system is in an unstable state, and the larger the sum is, the more unstable the system is.

### 4.1 Damping coefficient

Keeping the other control variables unchanged, the damping coefficient of the system is changed according to Table 2, and the time domain variation curve of the vibration power input function of the slider can be obtained by using the established friction pair model for calculation, as shown in Figure 7.

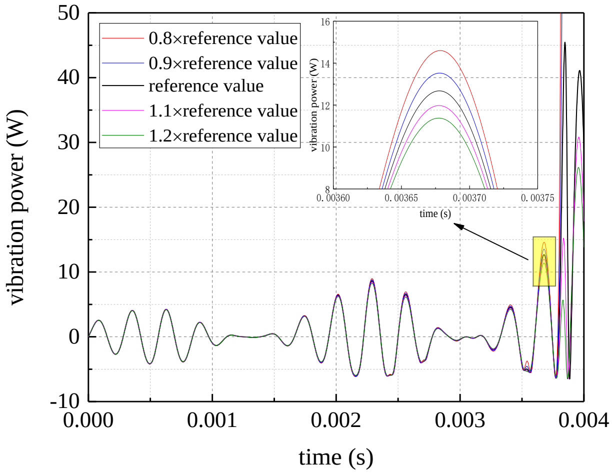


Fig. 7 Time domain curves of vibration power under different damping coefficients

As can be seen from Figure 7, with the increase of time, the sum of the slider vibration power corresponding to the five sets of damping coefficients in a fixed period is constant at 0 (the first period) or greater than 0 (the second and third periods), and the value of the sum gradually increases, that is, the system energy is increasing, indicating that the system is in an unstable stick-slip oscillation process. Meantime, as the increase of the damping coefficient, it is found that the variation amplitude of the slider vibration power decreases gradually, which illustrates that increasing the damping coefficient can minimize the phenomenon of unstable stick-slip oscillation.

## 4.2 Modal stiffness

Similarly, keeping the other variables unchanged, changing the modal stiffness of the system according to Table 2, and using the friction pair model for calculation, the time domain curve of the corresponding vibration power input function of the slider can be obtained, as shown in Figure 8.

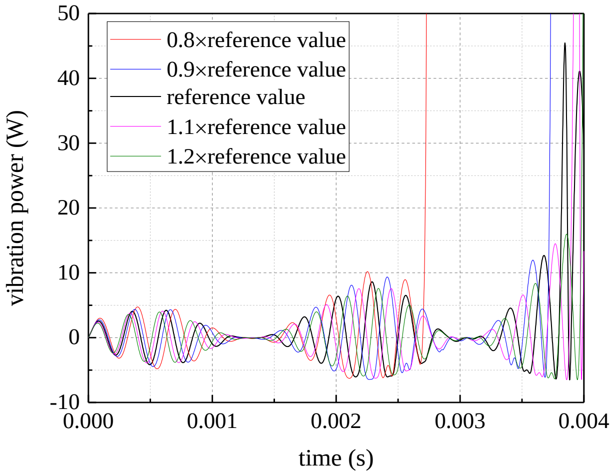


Fig. 8 Time domain curves of vibration power under different modal stiffnesses

According to Figure 8, with the increase of time, the sum of the slider vibration power corresponding to the five sets of modal stiffnesses in a fixed period is constant at 0 (the first period) or greater than 0 (the second and third periods), and the value of the sum keeps increasing, that is, the system energy keeps increasing, indicating that the system is in the process of unstable stick-slip oscillation. Moreover, by increasing the modal stiffness, it can be seen that the variation amplitude of the slider vibration power decreases gradually, which illustrates that the larger modal stiffness can also reduce the degree of unstable stick-slip oscillation. In addition, different from the condition of damping coefficient, the variation of modal stiffness will cause the phase change of the system stick-slip oscillation curve (i.e., the vibration power curve), so that the peak value of the stick-slip oscillation curve will be offset. This conclusion can be employed to control the degree of unstable stick-slip oscillation at a specific position.

### 4.3 Static vertical force

With the other variables unchanged, the static vertical force of the system is changed according to Table 2. Through calculation, the time domain variation curve of the corresponding vibration power input function of the slider can be obtained, as shown in Figure 9.

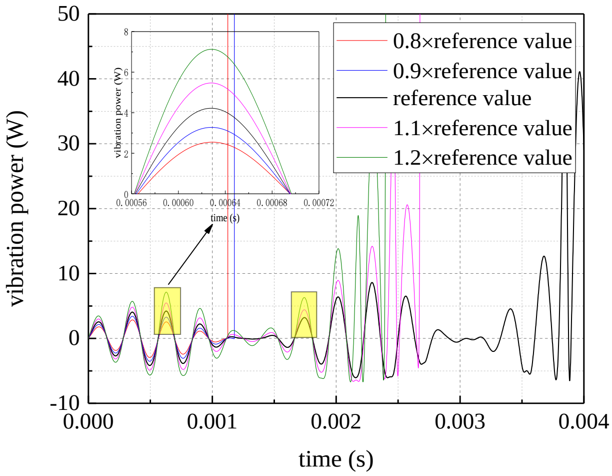


Fig. 9 Time domain curves of vibration power under different static vertical forces

It can be seen from Figure 9 that, with the increase of time, the sum of the slider vibration power corresponding to the five sets of static vertical forces in a fixed period is constant at 0 (the first period) or greater than 0 (the second and third periods), and the value of the sum continues to increase, indicating that the system energy is increasing continuously, that is, the system is in the process of unstable stick-slip oscillation. Meantime, with the increase of the static vertical force, the variation amplitude of the slider vibration power increases gradually at the fixed time, which demonstrates that the greater the static vertical force is, the more severe the degree of unstable stick-slip oscillation will be.

### 4.4 Lateral velocity (AoA)

By changing the lateral velocity (AoA) of the system according to Table 2 and keeping the other control variables unchanged, the time domain curve of the vibration power input function of the slider can be acquired through the model calculation, as shown in Figure 10.

According to Figure 10, it can be found that, with the increase of time, the sum of the slider vibration power corresponding to the five sets of lateral velocities (angles of attack) in a fixed period is constant at 0 (the first period) or greater than 0 (the second and third periods), and the value of the sum is increasing, indicating that the system energy is increasing continuously, and the system is in the process of unstable stick-slip oscillation. Furthermore, with the increase of the lateral velocity (AoA), the variation amplitude of the slider vibration power tends to decrease, and the degree of decrease gradually becomes slower, which illustrates that the degree of unstable stick-slip oscillation will gradually decrease with the increase of the lateral velocity (AoA).

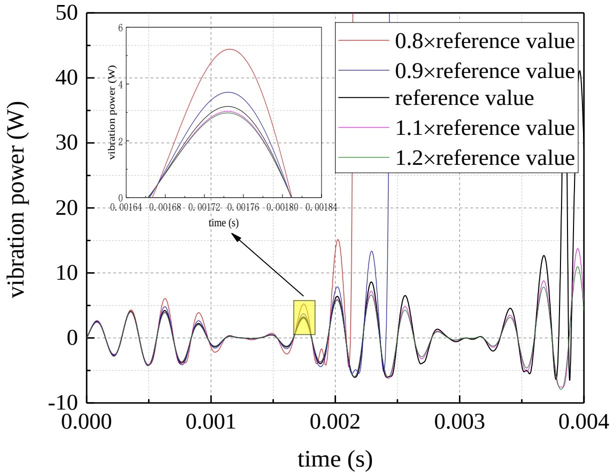


Fig. 10 Time domain curves of vibration power under different lateral velocities (angles of attack)

From the above, it can be seen that within a certain range, the phenomenon of unstable stick-slip oscillation can be effectively controlled by increasing the damping coefficient, increasing the modal stiffness, appropriately reducing the static vertical force of the contact interface and increasing the lateral velocity (AoA). The above conclusions can be further extended to the wheel-rail system, and because the variation of modal stiffness can cause the phase change of the system's stick-slip oscillation curve, the purpose of mitigating the degree of corrugation at the specific position on rail surface can be realized by changing the modal stiffness.

## CONCLUSIONS

Based on the actual wheel-rail motion relationship, a friction pair model considering different friction at-tributes is established. Then, the stick-slip oscillation features under various friction attributes are analyzed by using the model. Finally, the parameter analysis is carried out, including the damping coefficient, modal stiffness, static vertical force and lateral velocity, and the corresponding control measures for the stick-slip oscillation are proposed to slow down corrugation degree. The main conclusions are:

The lateral and vertical dynamics of the system play vital role on stick-slip oscillation characteristics. The negative slope friction creep property of the contact interface induces the unstable stick-slip oscillation, which increases the dynamic responses, while the positive slope friction creep property and zero slope friction creep property promote the stability of the system. Compared with the zero slope friction creep condition, the output variable amplitude increases by 119% to 1312% under the negative slope friction creep condition, and that decreases by 6% to 93% under the positive slope friction creep condition. In the sharp curve section, the formation of corrugation is mainly induced by the unstable stick-slip oscillation caused by the negative slope friction creep property of the contact interface. To avoid the negative slope friction creep property of the contact interface, the unstable stick-slip oscillation can be effectively suppressed, and the occurrence and evolution of rail corrugation can be controlled.

The parameter analysis shows that the unstable stick-slip oscillation can be effectively controlled by in-creasing the damping coefficient, increasing the modal stiffness, appropriately reducing the static vertical force of the contact interface and increasing the lateral velocity (AoA) within a certain range. Meanwhile, because the variation of modal stiffness can cause the phase change of the stick-slip oscillation curve, the purpose of reducing the rail corrugation at the determined position on rail surface can be achieved by changing the modal stiffness.

## REFERENCES


[1] Ramadan, M., Ahmet, S. "The mathematical analysis of demands for railway passenger transport in Kosovo", Strojnícky časopis – Journal of Mechanical Engineering 71 (2), pp. 189 – 198, **2021**. DOI: 10.2478/scjme-2021-0029

[2] Žiaran, S., Chlebo, O., Šooš, Ľ. "Methodology of prognostic vibro-acoustic analysis of buildings from potential dynamic loads generated by rail vehicles", Strojnícky časopis – Journal of Mechanical Engineering 73 (1), pp. 197 – 208, **2023**. DOI: 10.2478/scjme-2023-0016

[3] Li, W., Wang, H. Y., Wen, Z. F., Du, X., Wu, L., Li, X., Jin, X. S. "An investigation into the mechanism of metro rail corrugation using experimental and theoretical methods", Proceedings of the Institution of Mechanical Engineers, Part F: Journal of Rail and Rapid Transit 230 (4), pp. 1025 – 1039, **2016**. DOI: 10.1177/0954409715596182

[4] Fang, G., Wang, Y. R., Peng, Z. K., Wu, T. X. "Theoretical investigation into the formation mechanism and mitigation measures of short pitch rail corrugation in resilient tracks of metros", Proceedings of the Institution of Mechanical Engineers, Part F: Journal of Rail and Rapid Transit 232 (9), pp. 2260 – 2271, **2018**. DOI: 10.1177/0954409718769750

[5] Park, J., Ahn, A., Kim, J., Koh, Hyo-In., Park, J. "Direct determination of dynamic properties of railway tracks for flexural vibrations", European Journal of Mechanics-A/Solids 61, pp. 14 – 21, **2017**. DOI: 10.1016/j.euromechsol.2016.08.010

[6] Zhou, Z. J., Li, W., Wen, Z. F., Xiao, G. F. "Cause analysis of metro short-wavelength rail corrugation based on dynamic characteristics of wheel-rail surface", Journal of Vibration, Measurement and Diagnosis 40 (6), pp. 1040 – 1047, **2020**. DOI: 10.16450/j.cnki.issn.1004-6801.2020.06.002

[7] Balekwa, B. M., Kallon, D. V. V. "Correlation of short pitch rail corrugation with railway wheel-track resonance at low frequencies of excitation", Vibration 3 (4), pp. 491 – 520, **2020**. DOI: 10.3390/vibration3040031

[8] Pan, B., Wang, A. B., Gao, X. G., Liu, L. "Effect of lateral dynamic response characteristics of wheel-rail coupling systems on rail corrugation", Noise and Vibration Control 40 (1), pp. 132 – 137, **2020**. DOI: 10.3969/j.issn.1006-1355.2020.01.025

[9] Fourie, D., Fröhling, R., Heyns, S. "Railhead corrugation resulting from mode-coupling instability in the presence of veering modes", Tribology International 152, 106499, **2020**. DOI: 10.1016/j.triboint.2020.106499

[10] Beshbichi, O. El., Wan, C., Bruni, S., Kassa, E. "Complex eigenvalue analysis and parameters analysis to investigate the formation of railhead corrugation in sharp curves", Wear 450 – 451, 203150, **2020**. DOI: 10.1016/j.wear.2019.203150

[11] Chen, G. X., Zhou, Z. R., Ouyang, H., Jin, X. S., Zhu, M. H., Liu, Q. Y. "A finite element study on rail corrugation based on saturated creep force-induced self-excited vibration of a wheelset–track system", Journal of Sound and Vibration 329 (22), pp. 4643 – 4655, **2010**. DOI: 10.1016/j.jsv.2010.05.011

[12] Chen, G. X., Qian, W. J., Mo, J. L., Zhu, M. H. "A transient dynamics study on wear-type rail corrugation on a tight curve due to the friction-induced self-excited vibration of a wheelset-track system", Journal of Mechanical Engineering 50 (9), pp. 71 – 76, **2014**. DOI: 10.3901/JME.2014.09.071

[13] Yao, H. M., Shen, G., Gao, L. J. "Formation mechanism of worn profile rail corrugation based on experimental verification", Journal of Tongji University (Natural Science) 46 (10), pp. 1427 – 1432, **2018**. DOI: 10.11908/j.issn.0253-374x.2018.10.015

[14] Sun, Y. Q., Simson, S. "Wagon-track modelling and parametric study on rail corrugation initiation due to wheel stick-slip process on curved track", Wear 265 (9 – 10), pp. 1193 – 1201, **2008**. DOI: 10.1016/j.wear.2008.02.043

[15] Matsumoto, A., Sato, Y., Ono, H., Tanimoto, M., Oka, Y., Miyauchi, E. "Formation mechanism and countermeasures of rail corrugation on curved track", Wear 253 (1 – 2), pp. 178 – 184, **2002**. DOI: 10.1016/S0043-1648(02)00097-2

[16] Daniel, W. J. T., Horwood, R. J., Meehan, P. A., Wheatley, N. "Analysis of rail corrugation in cornering", Wear 265 (9 – 10), pp. 1183-1192, **2008**. DOI: 10.1016/j.wear.2008.02.030

[17] Wen, Z. F., Jin, X. S., Xiao, X. B., Zhou, Z. R. "Effect of a scratch on curved rail on initiation and evolution of plastic deformation induced rail corrugation", International Journal of Solids and Structures 45 (7 – 8), pp. 2077 – 2096, **2008**. DOI: 10.1016/j.ijsolstr.2007.11.013

[18] Jin, X. S., Wen, Z. F., Xiao, X. B. "Investigation into mechanism of initial rail corrugation formation at a curved track", Journal of Mechanical Engineering 44 (3), pp. 1 – 8 +15, **2008**. DOI: 10.3901/jme.2008.03.001

[19] Jin, X. S., Xiao, X. B., Wen, Z. F., Zhou, Z. R. "Effect of sleeper pitch on rail corrugation at a tangent track in vehicle hunting", Wear 265 (9 – 10), pp. 1163 – 1175, **2008**. DOI: 10.1016/j.wear.2008.01.028

[20] Jin, X. S., Wen, Z. F. "Effect of discrete track support by sleepers on rail corrugation at a curved track", Journal of Sound and Vibration 315 (1 – 2), pp. 279 – 300, **2008**. DOI: 10.1016/j.jsv.2008.01.057

[21] Xiong, J. Y., Jin, X. S. "Effects of lateral dent on curved rail on rail corrugation", Engineering Mechanics 23 (6), pp. 135 – 141 +134, **2006**. Available at: https://engineeringmechanics.cn/article/id/282

[22] Liu, X. G., Wang, P. "Investigation of the generation mechanism of rail corrugation based on friction induced torsional vibration", Wear 468 – 469, pp. 203593, **2021**. DOI: 10.1016/j.wear.2020.203593

[23] Cui, X. L., Chen, G. X., Zhao, J. W., Yan, W. Y., Ouyang, H. J., Zhu, M. H. "Field investigation and numerical study of the rail corrugation caused by frictional self-excited vibration", Wear 376-377, pp. 1919 – 1929, **2017**. DOI: 10.1016/j.wear.2017.01.089

[24] Cui, X. L., Huang, B., Du, Z. X., Yang, H. J., Jiang, G. "Study on the mechanism of the abnormal phenomenon of rail corrugation in the curve interval of a mountain city metro", Tribology Transactions 63 (6), pp. 996 – 1007, **2020**. DOI: 10.1080/10402004.2020.1782551

[25] Cuervo, P. A., Santa, J. F., Toro, A. "Correlations between wear mechanisms and rail grinding operations in a commercial railroad", Tribology International 82, pp. 265 – 273, **2015**. DOI: 10.1016/j.triboint.2014.06.025

[26] Liu, X. G., Xiao, C. B. "Investigation of the generation mechanism of squeal noise under non-negative damping conditions", Proceedings of the Institution of Mechanical Engineers, Part F: Journal of Rail and Rapid Transit 235 (7), pp. 887 – 897, **2021**. DOI: 10.1177/0954409720966467

[27] De Beer, F. G., Janssens, M. H. A., Kooijman, P. P. "Squeal noise of rail-bound vehicles influenced by lateral contact position", Journal of Sound and Vibration 267 (3), pp. 497 – 507, **2003**. DOI: 10.1016/S0022-460X(03)00710-7

[28] Popp, K., Schneider, E., Irretier, H. "Noise generation in railway wheels due to rail-wheel contact forces", Vehicle System Dynamics 15, pp. 448 – 466, **1986**. DOI: 10.1080/00423118508968829

[29] Shen, Z. Y., Hedrick, J. K., Elkins, J. A. "A comparison of alternative creep force models for rail vehicle dynamic analysis", Vehicle System Dynamics 12 (1 – 3), pp. 79 – 83, **1983**. DOI: 10.1080/00423118308968725

[30] Gorbunov, M., Kravchenko, K., Bureika, G., Gerlici, J., Nozhenko, O., Vaičiūnas, G., Bučinskas, V., Steišūnas, S. "Estimation of sand electrification influence on locomotive wheel/rail adhesion processes", Eksploatacja i Niezawodnosc-Maintenance and Reliability 21 (3), pp. 460 – 467, **2019**. DOI: 10.17531/ein.2019.3.12

[31] Shen, G., Zhang, X. H., Guo, M. H. "Theoretical study on rail corrugation on curved track of metro systems", Journal of Tongji University (Natural Science) 39 (3), pp. 381 – 384, **2011**. DOI: 10.3969/j.issn.0253-374x.2011.03.013

[32] Wang, Z. Q., Lei, Z. Y., Zhao, Y., Xu, Y. "Rail corrugation characteristics of cologne egg fastener section in small radius curve", Shock and Vibration 1827053, **2020**. DOI: 10.1155/2020/1827053